Paul S. Hammon, Scott Makeig, Howard Poizner, Emanuel Todorov, and Virginia R. de Sa

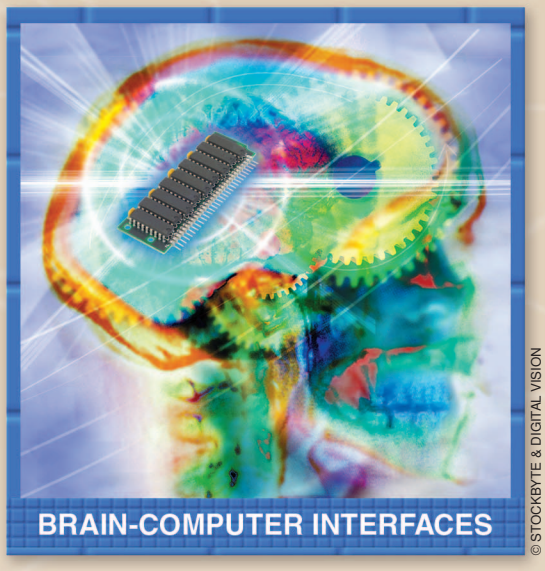

Predicting Reaching Targets from Human EEG

Laying the foundation

Extracting reach information from brain signals is of great interest to the fields of brain-computer interfaces (BCIs) and human motor control. To date, most work in this area has focused on invasive intracranial recordings; however, successful decoding of reach targets from noninvasive electroencephalogram (EEG) signals would be of great interest. In this article, we show that EEG signals contain sufficient information to decode target location during a reach (Experiment 1) and during the planning period before a reach (Experiment 2). We discuss the application of independent component analysis and dipole fitting for removing movement artifacts. With this technique we get similar classification accuracy for classifying EEG signals during a reach (Experiment 1) and during the planning period before a reach (Experiment 2). To the best of our knowledge, this is the first demonstration of decoding (planned) reach targets from EEG. These results lay the foundation for future EEG-based BCIs based on decoding of planned reaches.

Digital Object Identifier 10.1109/MSP.2007.909004

INTRODUCTION

BCIs are being developed for a variety of applications ranging from assistive technologies for patients with motor disabilities to entertainment devices. Across the wide range of applications, all BCI systems share the same set of underlying components, which can be broken down into three main segments: brain signal acquisition, brain state decoding, and computer-mediated performance of a task. Some BCIs decode the brain state into a set of discrete classes such as yes/no commands, while other BCIs decode continuous data such as a reaching trajectory.

ONE GOAL OF BCI RESEARCH IS TO DEVELOP SYSTEMS CAPABLE OF DECODING NEURAL REPRESENTATIONS OF NATURAL MOVEMENT PLANNING AND EXECUTION.

One goal of BCI research is to develop systems capable of decoding neural representations of natural movement planning and execution. The large number of degrees of freedom, high complexity, and speed of natural movement pose particular challenges to building BCI systems of this type. In order to deal with these constraints, researchers typically use arrays of intracranial electrodes. There are several types of intracranial electrodes ranging from intracortical electrodes which measure the firing patterns of a small number of neurons (single- or multi- unit recordings) to subdural or epidural electrodes measuring the local field potentials generated by dendritic currents in large numbers of nearby neurons (electrocorticography, or ECoG). Relative to less-invasive recording methods, intracranial electrodes allow for higher spatial resolutions but suffer from increased costs and risks associated with surgical implantation and maintenance of the electrode array. To date, the vast majority of research in this area has focused on intracranial recordings in nonhuman primates; however, noninvasive recording techniques such as the EEG offer benefits like improved safety and lower cost.

In this article, we analyze human EEG signals recorded from two different reaching tasks. We begin with data from a natural reaching task and show that reaching targets can be decoded from EEG. The promising results from this initial experiment led us to perform a second experiment based on a delayed reaching task. Results from this second experiment confirmed the findings from the first experiment and show that human EEG contains sufficient information to classify reaching targets even before movement has begun.

RECORDING BRAIN SIGNALS DURING REACHING

There is a large body of BCI research using signals from intracranial electrodes in monkeys during reaching tasks. For example, in [16] Serruya et al. demonstrate that intracortical single unit recordings from a small number of primary motor cortex neurons can be used to reconstruct movement trajectories without extensive subject training. Another study demonstrates that recordings from the parietal reach region can be used to detect high-level movement goals [11]. Furthermore, the BCI system with the highest information transfer rate to date [15] is based on implanted electrodes in macaques. Recent work with ECoG data recorded during human reaching tasks [14] indicates that reaching data can be decoded from cortical activity at lower spatial resolutions than in single unit recordings.

However, there is little work in this area using EEG data. There are two main reasons why EEG data is rarely used for reaching tasks. The first and perhaps most significant reason is due to contamination from artifacts. EEG electrodes sense all electrical activity at the scalp and therefore record not only electrical signals generated by brain activity but also electrical activity generated by eye movements and contraction of head and neck muscles. Therefore, experiments using EEG are typically designed to minimize any movement. In order to use EEG data during a task which involves movement, it is important to isolate and remove artifacts.

A second drawback of EEG is that it records the aggregate activity of large numbers of neurons. Thus, it is generally thought that EEG does not extract sufficiently detailed information to reconstruct complex movements.

Our goal is to show that—with appropriate artifact removal, signal processing, and machine learning—human EEG carries sufficient information about reach intention to decode reaching targets from the EEG signal during movement planning and execution.

EXPERIMENT 1

EEG and three-dimensional (3-D) movement data were simultaneously recorded during a cued reaching task in a darkened room. EEG data were sampled at 256 Hz using a 256-channel Biosemi ActiveTwo system with sintered Ag-AgCl active electrodes. Movement data were recorded using a Northern Digital, Inc. Optrack Certus 3-D tracking system. Three-dimensional locations of the hand, wrist, elbow, shoulder, and the three target LEDs were sampled at 250 Hz.

Subjects (four male, average age 44, all right-handed) sat in a comfortable chair and used their right index finger to reach for one of three target LEDs situated to the left (L), center (C), and right (R) of the subject's sternum. The LED targets differed in height and distance from the sternum and were positioned such that each subject could reach them without resorting to a full arm extension. Two different starting postures of the arm were used: one with the right forearm horizontal and the upper arm vertical (H), and the other with the right arm fully flexed with the forearm vertical (V). An individual trial began with LED illumination. Subjects were instructed to make an immediate and natural reach to the target. The LED stayed on until the target was touched, or for 2,500 ms in case of target miss. After touching the target, subjects were instructed to pause briefly and then return to the starting position. Target touch (or time out) was followed by a random interval of 800–1,200 ms before the next target appeared.

[TABLE 1] EXPERIMENT 1 SUBJECT MOVEMENT DATA (RELATIVE TO LED ONSET).

	RIGHT			CENTER			LEFT		
SUBJECT	PLAN	MOVE	TRIALS	PLAN	MOVE	TRIALS	PLAN	MOVE	TRIALS
S1	362	675	203	342	629	207	346	664	202
S2	297	443	205	267	394	214	283	416	196
S3	252	523	206	242	472	214	240	485	212
S4	303	721	183	288	645	192	256	642	207

Starting pose was blocked, with subjects randomly assigned the starting pose for the first half (either H or V), with the remaining pose used for the second half (either V or H). There were four different sequences of 20 pseudo-random reaching targets each. Each sequence was run four times per starting pose condition, for a total of 320 trials per starting pose, and 640 trials overall.

EXPERIMENT 1 DATA PREPROCESSING

The first step of data analysis was to reduce the dimensionality by cutting down the number of channels from 256 to 140 or 150. Channels with poor coupling or other problems were removed first, followed by channels located low on the head or neck, as these tend to have poor connections and large movement artifacts. Next channels were removed one at a time based on closest physical proximity to other electrodes until the desired number of channels (150 channels for S1, S3, and S4; 140 channels for S2) was met. Channel removal is a reasonable form of dimensionality reduction for high-density EEG because nearby channels are highly correlated, and thus little information is lost.

The EEG and movement data were aligned by re-sampling the movement data from 250 Hz to 256 Hz. The movement data were divided into two different segments: a planning segment (plan) from LED illumination until movement was detected, and a movement segment (move) consisting of forward movement to the target. Movement initiation was defined as the point at which the fingertip sensor reached 5% of the peak velocity during the initial acceleration phase. Termination of forward movement was defined as the point at which movement was at or near a minimum velocity and shifted direction, corresponding to the point in time at which the arm reversed direction and began returning to the starting position. Arm trajectories were visually inspected, and trials revealing data collection errors due to factors such as a subject starting a trial early or occluded LEDs were excluded from further analysis [13].

Movement data for the four subjects is summarized in Table 1 broken down by the three different reaching targets. Average times for both movement planning and execution are listed in ms. An average of 612 trials was analyzed for each of the four subjects.

EEG ARTIFACT DETECTION AND REMOVAL

EEG data recorded during eye or other muscle movement typically contain movement artifacts. Artifacts associated with eye movement occur because the eye has an uneven charge distribution and therefore acts as an electric dipole. Eye blinks and other movements generate a varying electrical field that propagates throughout the head and is picked up by scalp electrodes. Muscles generate electrical activity when they contract. Muscle tension in scalp, face, and neck muscles generates signals which also propagate throughout the scalp adding electromyographic (EMG) activity to electrodes near the muscle insertion.

The standard approach to handling artifacts in EEG research is to avoid them by developing experiments which restrict movement as much as possible, and then discarding trials which contain movement artifacts. This approach, however, is impractical for natural reaching tasks, in which eye and muscle movement are generally unavoidable.

Because reach data is especially susceptible to contamination from EEG artifacts that could potentially lead to erroneous classification rates, we employ an especially conservative artifact removal procedure, which is described in the following sections.

INDEPENDENT COMPONENT ANALYSIS

The first step of our artifact removal approach is to run independent component analysis (ICA) on the EEG data. ICA is a statistical technique which takes recordings from an array of sensors and determines a set of source signals which are maximally independent according to a specified measure of statistical independence. ICA posits a data model $X = AS$, where X are stacked row vectors of data recorded from individual sensors, A is a matrix of mixing weights, and S are the stacked row vectors of statistically independent source vectors. Given only the data X, the ICA algorithm returns estimates for both A and S: $\hat{S} = \hat{A}^{-1}X$. The vectors in $\hat{S}$ are termed "independent components" (ICs). The columns of $\hat{A}^{-1}$ indicate how to construct an individual IC as a weighted combination of channels of X. Thus, we can visualize the distribution of an IC over the scalp by plotting the values from a column of $\hat{A}^{-1}$ at each electrode location on the scalp to generate IC scalp maps (see Figure 1).

The ICA model assumes linear mixing of the sources as represented by the matrix A. Given a set of electrical sources in the brain, this linear mixing assumption holds because the net electrical potential between any two scalp electrodes is simply the superposition of the potentials resulting from each source.

There are a variety of ICA algorithms which primarily differ in the independence measure used. For artifact removal, we use InfoMax ICA [1], [9], which aims to minimize mutual information between sources by maximizing entropy. For ICA calculations and component visualization, we use EEGLAB [2].

ICA DIPOLE-BASED ARTIFACT REMOVAL

Once ICA components have been recovered, we attempt to fit dipoles to the IC scalp maps using the DIPFIT plug-in for

EEGLAB. This software package uses a four-shell spherical model (the brain, pial surface, skull, and scalp) and attempts to find either a single dipole or a pair of symmetric dipoles which best fit the IC scalp map. See [12] for details.

Each ICA component gets a dipole fit, but we only consider dipoles which are good fits ($<15\%$ residual variance between the IC scalp map and the fitting dipole scalp map). The location of the "good fit" dipoles are then checked against the head model, and only those dipoles which reside within the brain volume of the model are retained.

All ICA components which do not meet our diple requirements are removed. The ith ICA component can be removed by first zeroing out column i of the mixing matrix $\hat{A}$ to form a new matrix $\hat{A}_i$. Then the cleaned EEG data consisting of all but the removed component can be reconstructed as $X_i = \hat{A}_i S$.

OUR GOAL IS TO SHOW THAT—WITH APPROPRIATE ARTIFACT REMOVAL, SIGNAL PROCESSING, AND MACHINE LEARNING—HUMAN EEG CARRIES SUFFICIENT INFORMATION ABOUT REACH INTENTION TO DECODE REACHING TARGETS FROM THE EEG SIGNAL DURING MOVEMENT PLANNING AND EXECUTION.

The EEG data generated by back-projecting only the good fit ICA components with equivalent dipoles located within the brain will be referred to as cleaned EEG. The scalp maps of the retained components for each of the four Experiment 1 subjects are shown in Figure 1.

FEATURE EXTRACTION

From the cleaned EEG data we extract a set of eight different feature vectors which were useful for classification in previous BCI work [4].

FEATURE 1: AUTOREGRESSIVE MODELING

An autoregressive (AR) system can be described by the difference equation $y(t) = -\sum_k a_k y(t-k) + w(t)$, where $w(t)$ is a white-noise random process and a_k are the autoregressive coefficients. Thus, an AR system can be thought of as white noise passed through an all-pole filter. AR models give a decent first-order approximation of real EEG spectra but require far less data than high-resolution FFTs [17]. We use a 3rd order model and compute AR coefficients using the Burg method [10], parameters which we found to work well in previous analysis [4]. This results in a feature vector with three feature values per channel.

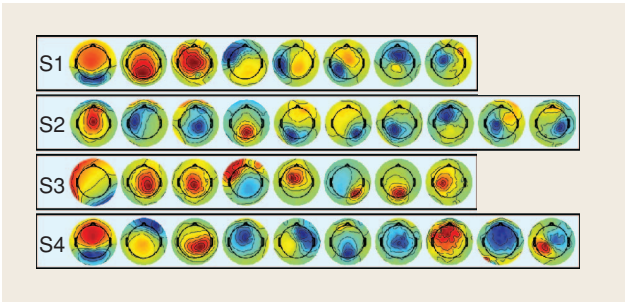

[FIG1] Scalp maps of the retained ICA components for all four Experiment 1 subjects. The hemispherical electrode locations are mapped to a flat disc, and thus electrodes further down on the head appear beyond the borders of the head outline.

FEATURE 2: POWER ESTIMATES USING A FILTER BANK

A different approach to generating spectral estimates is to use a bank of filters to determine power estimates over frequency ranges corresponding to the individual filters. This approach has added flexibility over direct FFT approaches and allows for shorter filters where lower resolution is sufficient. We create a bank of 9th order finite impulse response (FIR) filters over the following frequency bands: delta (1–3 Hz), theta (4–7 Hz), alpha/mu (8–13 Hz), beta (14–25 Hz), and gamma (26–40 Hz). To generate the power estimate over a single frequency band, we filter the data, perform a point-wise squaring of the filtered signal, and finally compute the mean. This yields five feature values per channel.

FEATURE 3: CLEANED EEG DATA

The cleaned EEG data is the starting point for all features and thus contains all available (artifact-rejected) information about the user's brain state; however, the dimensionality of the data is too high. In order to reduce dimensionality, we re-sample the data to a fixed length of ten samples per channel.

FEATURE 4: DISCRETE WAVELET TRANSFORM

The discrete wavelet transform (DWT) offers a middle ground between frequency-based and time-based representations. We include a Symlet-based three-level DWT decomposition, which is applied to the data and then re-sampled to a total of 10 samples per channel.

FEATURES 5–8: ICA TRANSFORMS

Features 5–8 are generated by performing an ICA decomposition of the cleaned EEG data and then applying features 1–4, respectively. Feature 7 was resampled to eight rather than the intended ten points. Subsequent analysis with ten point resampling yielded results very similar to those reported here. Although InfoMax ICA was run on the complete dataset for artifact removal, we did not use these ICA components for our feature vectors because they are computed using the complete dataset, and for the classification stage we want to predict performance on future data not in our training dataset. Because of this, we built a separate ICA decomposition into our classification cross-validation loops and trained only on the current training segment. Computation speed is important for classifier training, so features 5–8 use a FastICA [5] decomposition because it can be computed more

[TABLE 2] CLASSIFICATION ERROR RATES (± STANDARD DEVIATION) FOR TARGET REACHING.

	TARGET END POINT (THREE-CLASS)		STARTING POSE (TWO-CLASS)	
SUBJECT	**PLAN**	**MOVE**	**PLAN**	**MOVE**
S1	0.502 ± 0.0705	0.459 ± 0.0415	0.0572 ± 0.0222	0.0147 ± 0.00327
S2	0.369 ± 0.0421	0.380 ± 0.0314	0.163 ± 0.0325	0.125 ± 0.0243
S3	0.342 ± 0.0301	0.263 ± 0.0285	0.0158 ± 0.0121	0.0142 ± 0.0108
S4	0.433 ± 0.0448	0.378 ± 0.0361	0.0533 ± 0.0249	0.0275 ± 0.0110

rapidly [6] than InfoMax ICA, which was used in the artifact removal stage. Due to the reduced rank of the cleaned EEG data, this application of ICA yields the same number of ICA components as were retained in artifact removal—eight for S1 and S3, and ten for S2 and S4.

CLASSIFICATION APPROACH

Our classification approach involves creating individual classifiers based on each of the eight different feature vectors, and then combining these individual classifiers into a meta-classifier [4]. Classifier training takes place in a nested cross-validation scheme. An outer four-fold cross-validation loop segments the data into training (75%) and test (25%) sets. This outer loop runs four times such that each sample is a member of the test set exactly once. Eight individual classifiers are trained inside this loop. Within each outer cross validation loop, there is a two-fold inner cross-validation loop in which the (outer) training data is once again segmented into (inner) training (50%) and test (50%) data. This inner cross validation loop is used to select classifier regularization parameters (described later). The individual classifiers are combined into a meta-classifier which is then tested on the test data. This procedure is outlined below.

1) outer cross-validation loop $i = 1:4$
   a) loop over features $j = 1:8$
      i) extract feature j
      ii) inner cross-validation loop $k = 1:2$
         A) loop over regularization parameters $k = 1:7$
      iii) select best regularization parameter λ
      iv) train classifier on feature j with regularization parameter λ
   b) combine individual classifiers to create meta-classifier i
   c) compute classification rate on test data i
2) compute average cross-validation classification rate.

MULTINOMIAL LOGISTIC CLASSIFICATION

There are a variety of different classification approaches currently in use with BCI data. It is becoming increasingly clear that many different classifiers perform well given a sufficiently rich feature set [4]. This particular application has high-dimensional multiclass data. Thus, we would like to use a classifier with regularization to avoid over-fitting and native multiclass support to avoid training multiple one-versus-rest classifiers. To address these two characteristics, we use sparse multinomial logistic regression [8].

The multinomial logistic regression classifier is:

$$p(y^{(i)} = 1 | \boldsymbol{x}; \boldsymbol{w}) = \frac{\exp\left(\boldsymbol{w}^{(i)^T}\boldsymbol{x}\right)}{\sum_{j=1}^{m} \exp\left(\boldsymbol{w}^{(j)^T}\boldsymbol{x}\right)}, \quad (1)$$

where i indicates the class number, $y^{(i)}$ is 1 for class i and 0 otherwise, $\boldsymbol{x}$ is the feature vector, $\boldsymbol{w}^{(i)}$ is the weight vector for class i, and m is the number of classes.

The regularization comes from placing a sparsity-promoting Laplacian prior on the weight vectors $\boldsymbol{w}^{(i)}$:

$$p(\boldsymbol{w}^{(i)}) \propto \exp(-\lambda \|\boldsymbol{w}^{(i)}\|_1), \quad (2)$$

where λ is a regularization parameter and $\|\cdot\|_1$ denotes the l_1 norm. We use the inner cross-validation loop to select the best value of λ from $\{0, 10^{-6}, 10^{-4}, 10^{-2}, 10^{0}, 10^{2}, 10^{4}\}$.

COMBINING CLASSIFIERS

Combining multiple classifiers has the potential of reducing error rates both by reducing variance and by combining possibly independent types of information [3], [4]. We combine the output of the eight individual classifiers using an average meta-classifier: average the predicted probabilities for each class across all individual classifiers, and the class with the highest average probability is selected as the predicted class output. The average meta-classifier is robust to individual classifiers with poor probability estimates [7], and it has no parameters, which avoids extra steps for tuning the meta-classifier parameters.

EXPERIMENT 1 CLASSIFICATION RESULTS AND FEATURE ANALYSIS

We built classifiers to investigate two different aspects of the combined movement and EEG data: two-class classifiers to determine starting pose collapsed across target end points, and three-class classifiers to determine target end point collapsed across starting positions. We built separate classifiers for each of the two different data segments, plan and move. Average cross-validation results are summarized in Table 2.

Reaching target error rates were somewhat high for the plan segment (ranging from 34% to 50% error) and generally lower for the move segment (ranging from 26% to 46% error). While these error rates may seem somewhat high, they are all well below chance (67%), and half of the subjects tested had error rates in the 30% error range. These relatively high error rates may be at least partially due to the conservative artifact rejection

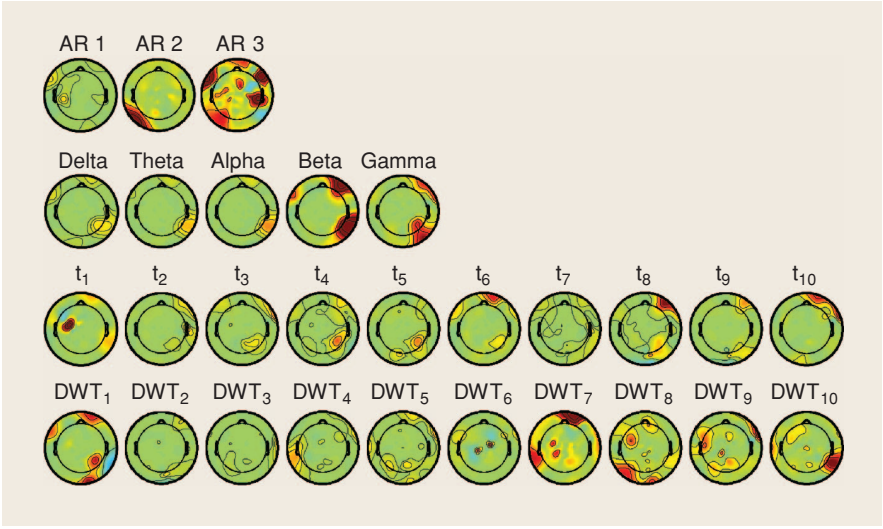

[FIG2] **Scalp maps of feature importance averaged across all four Experiment 1 subjects.**

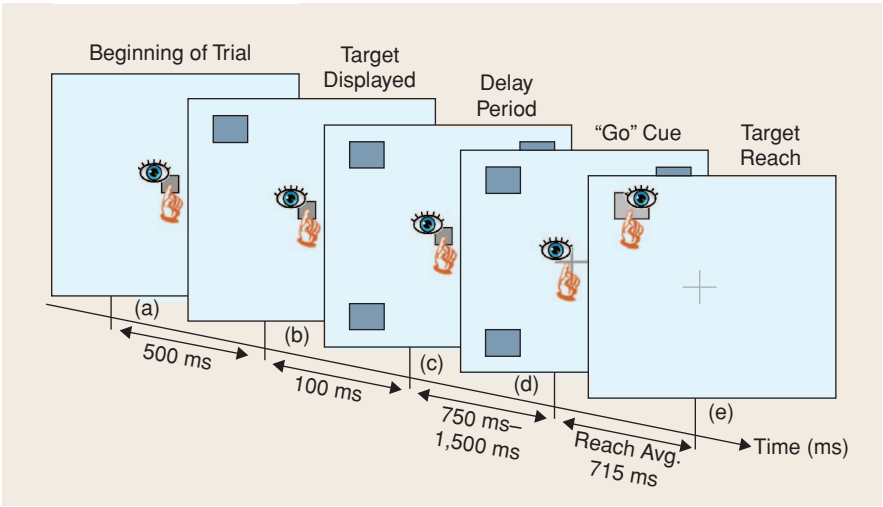

[FIG3] **A single trial from Experiment 2.**

scheme that reduced the rank of the EEG data from 150 (140 for S2) down to 8–10 ICA components.

It is worth noting that the starting pose is more discriminable than the three different reaching targets. This is not too surprising, as these two poses differ more than any pair of poses from reaches to different targets. However, the error rates on the order of 1% are somewhat suspicious. One possibility is that the high classification rates are at least partially due to the nature of the experimental design, in which all trials from a given starting pose were run as a block. Thus, starting pose could act as a proxy for first versus second half of the experiment.

To better understand what specific aspects of brain activity were most important for target reach classification, we investigated the individual classifiers. One way to do this is to analyze trained classifier weights, which indicate the relative importance of the corresponding features. To compare feature weights across subjects, we constructed a reduced set of 69 channels which matched locations across all four subjects, scaled each feature vector to have the same average length, and only analyzed the channel-based features 1–4, which could be lined up across subjects.

To visualize the feature weights, we took the feature weights (from the plan stage) and averaged across cross-validation folds and subjects. For each feature, this gives three weight vectors (one per class) which we reduced to a single vector by computing the variance across the three different classes. These values were then mapped onto 2-D head images using a fixed color map range for each feature. Results are shown in Figure 2. Each row represents a complete feature vector, with an average scalp map for each frequency/time feature.

The locations of the largest feature weights vary substantially in position across the four subjects and the different feature vectors. One feature of note is the large weights over left sensorimotor areas (t_1, AR_1), which lie near the hand area of primary motor cortex contralateral to the reaching hand. Some features show large weights over frontal areas (beta, gamma, DWT_7). These could be due to frontal attention processes, but it is also possible that these are due to remnant eye artifacts. The occipital and temporal weights (beta, gamma, DWT_1, DWT_{10}) could be related to visual processing, but lie in an area which could also suggest neck muscle artifacts. All features showed large differences across subjects, reinforcing the notion that tailoring classifiers to each individual is crucial for good BCI performance.

EXPERIMENT 2

The results from Experiment 1 are encouraging; however, while our artifact rejection scheme should remove most eye and muscle artifacts, it is possible that some artifact information was not successfully rejected and affected the classification results. Thus, we developed and ran a second experiment in which we had greater control over potential EEG artifacts.

Our second experiment is a center-out delayed reaching task modeled after the delayed reaching task employed by Santhanam et al. in [15]. In our variation, the subject sits back in a comfortable chair positioned within easy reaching distance of a 19-in LCD touch screen (Elo TouchSystems Model 1925L). EEG data were recorded at 256 Hz using a 64-channel Biosemi

ActiveTwo system with sintered Ag-AgCl active electrodes. Two subjects were run in this new paradigm, one who also participated in Experiment 1 (S2: male, age 58, right-handed) and one new subject (S5: female, age 27, right-handed).

[TABLE 3] EXPERIMENT 2 SUBJECT DATA AND RESULTS.

		CLASSIFICATION ERROR RATES (± STANDARD DEVIATION)		
SUBJECT	TRIALS	4-CLASS	LEFT VERSUS RIGHT	TOP VERSUS BOTTOM
S2	544	0.439 ± 0.0645	0.265 ± 0.0708	0.313 ± 0.0272
S5	536	0.414 ± 0.0325	0.142 ± 0.0305	0.326 ± 0.0347

A single trial of the experiment is diagramed in Figure 3. Subjects are instructed to touch, hold, and fixate on a central target [Figure 3(a)]. After a short delay, a reach target briefly appears (100 ms) in one of the four corners of the screen [Figure 3(b)]. All four possible targets are then shown and the experiment begins a variable delay phase (randomly selected between 750 ms and 1,500 ms) during which the subject maintains touch and fixation of the central fixation [Figure 3(c)]. After the variable delay, a "go" cue is indicated by replacing the central rectangular target with a cross [Figure 3(d)]. At this point, the subject performs a natural reach to the (remembered) correct target [Figure 3(e)]. In order to keep the reach as natural as possible, the subjects were not instructed to maintain central fixation during the actual reach. Touching the correct target before reach timeout (3 s) results in a "ding," while an incorrect reach or timeout is signaled by a "buzz."

A total of 800 trials were run for each subject with short breaks every 25 trials. The four targets were presented in pseudorandom order with a total of 200 trials for each target.

EXPERIMENT 2 DATA PREPROCESSING

The EEG data in this experiment were processed in exactly the same manner as those from Experiment 1, with only a few minor differences noted below. We used exactly the same algorithms for artifact removal, feature extraction, and classification. The differences noted below stem primarily from the different number of channels and different time course of this experiment. Scalp maps of the retained components for both Experiment 2 subjects are shown in Figure 4.

For Experiment 2, we only analyzed the first 500 ms of the delay period [Figure 3(d)]. During this period the visual stimulus is identical for all trials and visual fixation and arm position are held fixed. This segment was selected to minimize artifacts associated with eye and arm movements and systematic posture changes. Trials with incorrect target selection or reach timeout were excluded. The horizontal and vertical electrooculogram (HEOG and VEOG, respectively) were visually inspected, and any trials showing blink or eye movements were excluded. Before classifying the data, we randomly selected a balanced number of trials from each class. The numbers of trials analyzed is summarized in Table 3.

EXPERIMENT 2 RESULTS AND FEATURE ANALYSIS

Three different classifiers were constructed for each subject: a four-class classifier for reaching target, and two-class classifiers dividing the target space into left versus right reaches and top versus bottom reaches. Average cross-validation results are summarized in Table 3.

Both subjects had similar error rates in four-class target decoding, with both well below chance (75%). The two-class data showed an interesting pattern where classifiers for both subjects were substantially better at discriminating left from right targets than at discriminating top from bottom targets. These results are encouraging and further support our finding that reach targets can be successfully decoded from human EEG.

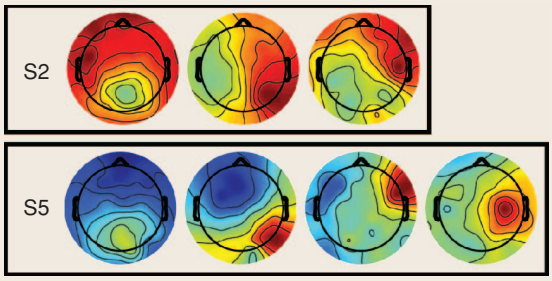

[FIG4] Scalp maps of the retained ICA components for both Experiment 2 subjects.

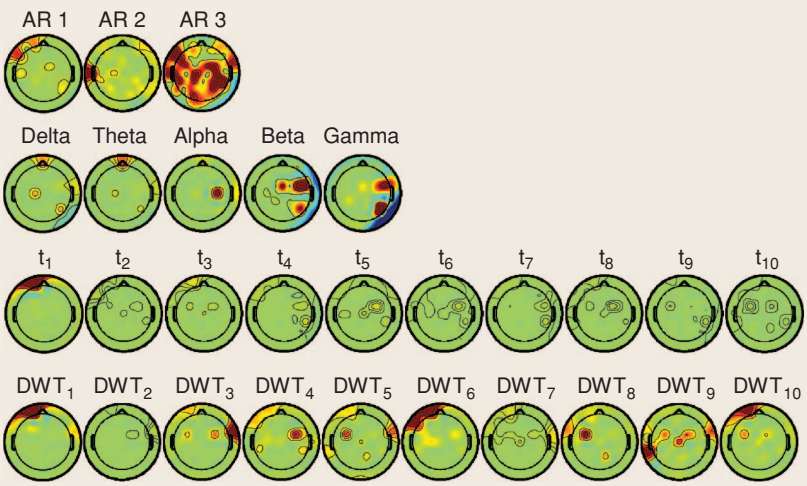

[FIG5] Scalp maps of feature importance averaged across Experiment 2 subjects.

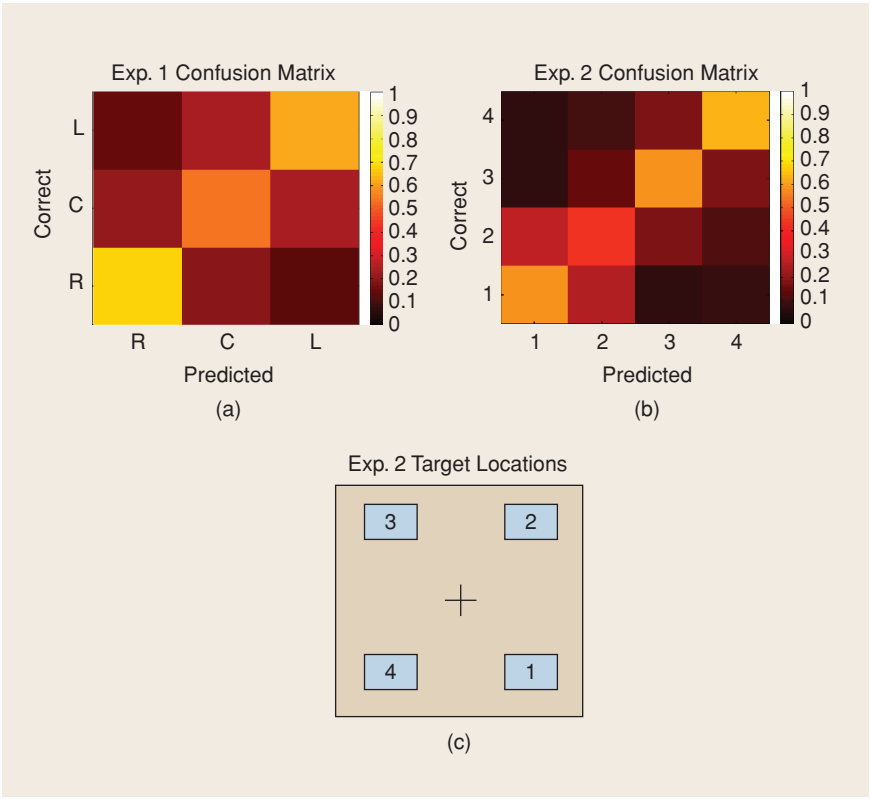

[FIG6] Average confusion matrices for (a) Experiment 1 and (b) Experiment 2 . These matrices illustrate what fraction of the data was classified as each of the possible predicted class labels. Lighter shades indicate larger fractions. Target labels for Experiment 2 are shown in (c).

We analyzed the features from Experiment 2 exactly the same way as in Experiment 1. The resultant feature maps are shown in Figure 5. Once again, weights vary substantially across subjects and features. Several features showed large weights over left and right sensorimotor areas (delta, alpha, $DWT_{3,4,5,8}$) which would be consistent with reach planning. Note that there is little activity over occipital/parietal regions (with the possible exception of gamma), suggesting that any neck muscle artifacts had little impact on classification. There are some large frontal weights (t_1, $DWT_{1,6,10}$) which might correspond to frontal attention processes. These could be eye artifacts, but this is less likely than in Experiment 1 because all trials with apparent eye movements were removed.

ERROR PATTERNS

One particularly interesting question about the EEG/movement data is whether or not it contains an underlying structure. One way such a structure might manifest itself is through structured errors. For example, in Experiment 1 one might expect that misclassified L trials are more likely to be (incorrectly) classified as C trials than R trials. To test this, we constructed confusion matrices for target endpoints for Experiments 1 and 2.

The average confusion matrix for Experiment 1 is shown in Figure 6(a), and the confusion matrix for Experiment 2 is shown in Figure 6(b). Rows indicate the correct class label, and columns indicate the predicted class label. Thus, each cell shows what fraction of examples from the row class was predicted to belong to the column class. For example, in Figure 6(a) row 1, column 2 (correct: L, predicted: C) shows the fraction of L trials which the classifier predicted to belong to class C in Experiment 1.

The structure of the Experiment 1 confusion matrix reveals that trials are most likely to be correctly classified, less likely to be misclassified one target away, and least likely to be misclassified two targets away. The Experiment 2 confusion matrix has a more complex structure suggesting that targets are most likely to be misclassified as nearby targets, but targets on the left (3, 4) are unlikely to be misclassified as targets on the right (1, 2), and vice-versa. These results suggest that there is an underlying structure to the target space, whereby targets nearby in physical space are also nearby in EEG feature space, but this target space may have additional complexities as it does in Experiment 2.

CONCLUSIONS

This article represents the first steps towards developing BCIs based on EEG recorded during reaching tasks. We described and applied an artifact removal approach suitable for EEG recorded during natural movements. In Experiment 1, we were able to remove movement artifacts from EEG recorded during a natural reaching task and use the cleaned EEG to successfully classify reaching targets. In Experiment 2, we decoded reaching targets using short segments of EEG from the premovement planning stage of a delayed reaching task.

We believe that our conservative artifact removal scheme should be sufficient to remove most movement-related EEG artifacts. This conjecture is supported by good classification performance on our delayed reaching task in Experiment 2, suggesting that our classification results on the natural reaching task in Experiment 1 are due to brain activity and not merely motion artifacts. The fact that the cleaned EEG data, especially in the planned reaching task, contained sufficient information to interpret the planned reach targets indicates that:

1) properly cleaned EEG is a viable data source for studying brain dynamics during reaching, and
2) EEG-based BCIs may be able to decode and act on desired reach commands.

ACKNOWLEDGMENTS

We thank Julie Onton and Miro Enev for assistance with movement decoding and data analysis, and Andrey Vankov for assistance with data acquisition.

This work was supported in part by NSF grant DGE-0333451 and NSF CAREER Award 0133996, a grant from the Kavli Brain-Mind Institute at UCSD, the Temporal Dynamics of Learning Center (NSF grant SBE-0542013), and NIH grant 2 R01 NS36449.

EYE BLINKS AND OTHER MOVEMENTS GENERATE A VARYING ELECTRICAL FIELD THAT PROPAGATES THROUGHOUT THE HEAD AND IS PICKED UP BY SCALP ELECTRODES.

AUTHORS

Paul S. Hammon (phammon@ucsd.edu) received a B.S. in electrical engineering in 2003, an M.S. in electrical engineering in 2005 (specializing in intelligent systems, robotics, and control), and is pursuing a Ph.D. in electrical engineering, all from the University of California at San Diego (UCSD). His main research interests include signal processing and machine learning applied to neural signals.

Scott Makeig (smakeig@ucsd.edu) is a research scientist at UCSD and director of the Swartz Center for Computational Neuroscience of UCSD. He has worked on EEG research for over twenty years, pioneering studies of auditory steady-state response dynamics, time-frequency analysis, and independent component analysis. His research focuses on observing and modeling how functional activities in multiple brain areas interact dynamically to support human awareness, interaction and creativity. His article, "Dynamic Brain Sources of Visual Evoked Responses," in *Science* (2002) has sparked renewed debate over the relevance of phase resetting of ongoing EEG activity to average event-related potentials.

Howard Poizner (hpoizner@ucsd.edu) is a research professor at the Institute of Neural Computation, and Adjunct Professor of Cognitive Science, UCSD. Prior to joining UCSD, he was Professor II of Neuroscience at Rutgers University, and before that, Associate Director of the Cognitive Neuroscience Laboratory at the Salk Institute for Biological Studies in La Jolla, California. He is the 2002 recipient of the Rutgers University Board of Trustees Excellence in Research Award. His research interests include motion analysis of patients with motor disorders and the brain dynamics that underlie motor control.

Emanuel Todorov (todorov@cogsci.ucsd.edu) received his Ph.D in cognitive neuroscience from Massachusetts Institute of Technology in 1998. He is now Assistant Professor of Cognitive Science at UCSD. His research focus is on biological movement, in particular using stochastic optimal control and Bayesian inference to understand how the brain does sensorimotor integration.

Virginia R. de Sa (desa@cogsci.ucsd.edu) received her Ph.D. in computer science from the University of Rochester. She did postdoctoral work under an NSERC fellowship at the University of Toronto and at the University of California at San Francisco in theoretical neurobiology as a Sloan Fellow. She joined the Department of Cognitive Science at UCSD in 2001 and is a member of the interdisciplinary programs in neuroscience, computational neuroscience, and cognitive science. Her interests include using machine learning methods to analyze neural signals, creating brain-motivated machine learning algorithms, and creating models of visual processing.

REFERENCES

[1] A.J. Bell and T.J. Sejnowski, "An information-maximization approach to blind separation and blind deconvolution," *Neural Comput.*, vol. 7, no. 6, pp. 1129–1159, 1995.

[2] A. Delorme and S. Makeig, "EEGLAB: An open source toolbox for analysis of single-trial EEG dynamicss," *J. Neurosci. Methods*, vol. 134, no. 2, pp. 9–21, 2004.

[3] G. Dornhege, B. Blankertz, G. Curio, and K.-R. Müller, "Boosting bit rates in noninvasive EEG single-trial classifications by feature combination and multiclass paradigms," *IEEE Trans. Biomed. Eng.*, vol. 51, no. 6, pp. 993–1002, 2004.

[4] P.S. Hammon and V.R. de Sa, "Pre-processing and meta-classification for brain-computer interfaces," *IEEE Trans. Biomed. Eng.*, vol. 54, no. 3, pp. 518–525, 2007.

[5] J. Hurri, H. Gävert, J. Särelä, and A. Hyvärinen, FastICA Package for Matlab, 2005. [Online]. Available: http://www.cis.hut.fi/projects/ica/fastica/code/dlcode.shtml

[6] A. Hyvärinen, J. Karhunen, and E. Oja, *Independent Component Analysis*. Wily, New York, 2001.

[7] J. Kittler, M. Hatef, R.P.W. Duin, and J. Matas, "On combining classifiers," *IEEE Trans. Pattern Anal. Machine Intell.*, vol. 20, no. 3, pp. 226–239, 1998.

[8] B. Krishnapuram, L. Carin, M.A.T. Figueiredo, and A.J. Hartemink, "Sparse multinomial logistic regression: Fast algorithms and generaliza-tion bounds," *IEEE Trans. Pattern Anal. Machine Learning*, vol. 27, no. 6, pp. 957–968, 2005.

[9] S. Makeig, A.J. Bell, T.-P. Jung, and T.J. Sejnowski, "Independent component analysis of electroencephalographic data," in *Advances in Neural Information Processing Systems 8,* D. Touretzky, M. Mozer, and M. Hasselmo, Eds. Cambridge, MA: MIT Press, 1996, pp. 145–151.

[10] S. Lawrence Marple, *Digital Spectral Analysis: With Applications*. Englewood Cliffs, NJ: Prentice- Hall, 1987.

[11] S. Musallam, B.D. Corneil, B. Greger, H. Scherberger, and R.A. Andersen, "Cognitive control signals for neural prosthetics," *Science*, vol. 305, pp. 258–262, July 2004.

[12] J. Onton and S. Makeig, "Information-based modeling of event-related brain dynamics," *Prog. Brain Res.*, vol. 159, pp. 99–120, 2006.

[13] H. Poizner, L. Mack, M. Verfaellie, L.J.G. Rothi, and K.M. Heilman, "Three-dimensional computergraphic analysis of apraxia," *Brain*, vol. 113, no. 1, pp. 85–101, 1990.

[14] J.C. Sanchez, A. Gunduz, P.R. Carney, and J.C. Principe, "Extraction and localization of mesoscopic motor control signals for human ECoG neuroprosthetics," *J. Neurosci. Methods*, doi:10.1016/j.jneumeth.2007.04.019, 2007.

[15] G. Santhanam, S.I. Ryu, B.M. Yu, A. Afshar, and K.V. Shenoy, "A high-performance brain-computer interface," *Nature*, vol. 442, pp. 195–198, July 2006.

[16] M.D. Serruya, N.G. Hatsopoulos, L. Paninski, M.R. Fellows, and J. Donoghue, "Brain-machine interface: Instant neural control of movement signal," *Nature*, vol. 416, pp. 141–142, Mar. 2002.

[17] J.R. Wolpaw, N. Birbaumer, D.J. McFarland, G. Pfurtscheller, and T.M. Vaughan, "Brain-computer interfaces for communication and control," *Clinical Neurophys.*, vol. 113, no. 6, pp. 767–791, 2002.

SP